

# Studies of measuring Higgs self-coupling with $HH \rightarrow b\bar{b}\gamma\gamma$ at the future hadron colliders

Weiming Yao<sup>\*1</sup>

<sup>1</sup>LBNL, Berkeley CA 94720, USA

We present a feasibility study of observing  $HH \rightarrow b\bar{b}\gamma\gamma$  at the future hadron colliders with  $\sqrt{s} = 14, 33$ , and 100 TeV. The measured cross section then can be used to constrain the Higgs self-coupling directly in the standard model. Any deviation could be a sign of new physics. The signal and background events are estimated using Delphes 3.0.10 fast Monte Carlo simulation based on the ATLAS detector capabilities. With  $3 \text{ ab}^{-1}$  data, it would be possible to measure the Higgs self-coupling with a 50%, 20%, and 8% statistical accuracy by observing  $HH \rightarrow b\bar{b}\gamma\gamma$  at  $\sqrt{s} = 14, 33$ , and 100 TeV colliders, respectively.

PACS numbers:

## I. INTRODUCTION

The ATLAS and CMS have recently discovered a new boson with a mass near 125 GeV/ $c^2$  [1], which is a giant leap for science. The updated results are consistent with the expectation of a Higgs boson [2], the missing cornerstone of particle physics. In order to directly test whether the Higgs mechanism is responsible for the electroweak symmetry breaking, we need to determine the Higgs self-coupling constants  $\lambda_{HHH}$  directly from data by observing the double Higgs production process  $gg \rightarrow H \rightarrow HH$ . In the standard model (SM), the Higgs self-coupling  $\lambda_{HHH}$  is equal to  $3M_H^2/v$  where  $v = 246 \text{ GeV}$  and  $M_H$  is the measured Higgs boson mass. An accurate test of this relation may reveal the extended nature of the Higgs sector, which can be achieved by observing a significant deviation from the SM prediction above [3–6]. Recent studies indicate that observing  $gg \rightarrow H \rightarrow HH$  is challenging at the high luminosity run of LHC (HL-LHC) with an integrated luminosity of  $3000 \text{ fb}^{-1}$  [7], due to destructive interference between  $HHH$  and  $gg \rightarrow HH$  processes that are shown in Fig. 1 (left).

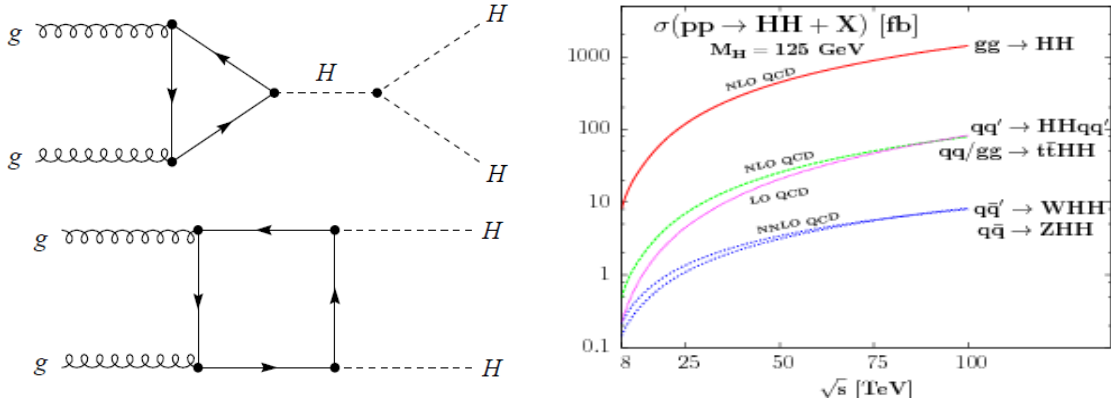


FIG. 1: The Feynman diagrams for the  $gg \rightarrow HH$  processes (left) and the corresponding production cross section as function of the collider energy  $\sqrt{s}$  (right).

In this study we study how feasible it is to measure Higgs self-coupling at the LHC and the future higher energy colliders (VLHC). We will focus on  $HH \rightarrow b\bar{b}\gamma\gamma$  as the baseline. The advantage of measuring the Higgs self-coupling at the higher energy colliders is their large production cross section rate as shown in Fig. 1 (right), which increases

\* Email contact: wmyao@lbl.gov

from 34 fb to 1418 fb when increasing the center mass of energy from 14 to 100 TeV [6]. Recent studies indicate that the resummation effects will further increase the NLO cross section by 20%-30% and reduce the scale uncertainties [8], which would improve the chance of measuring the Higgs self-coupling at HL-LHC.

## II. SIMULATION SETUP

Following the community summer studies 2013 (CSS 2013) guidelines, we use Delphes [9] V3.0.10 to simulate the ATLAS detector responses. More specifically, the photon energy is smeared according to the electromagnetic calorimeter (Ecal) responses of  $\sigma_{E_T}/E_T = 0.20/\sqrt{E_T} \oplus 0.17\%$ . The jet is clustered using the anti- $K_T$  algorithm with a radius of 0.5. The  $b$ -tagging operation point is chosen to have 75% of efficiency and 1% of mistags. In Fig. 2, we show the identification efficiencies for photons and  $b$ -jets as a function of  $Pt$  as well as the invariant mass distributions for  $H \rightarrow \gamma\gamma$  and  $H \rightarrow b\bar{b}$ , respectively. The photon identification efficiency is about 80% for photon with  $E_T > 25$  GeV and  $|\eta| < 2.5$ .

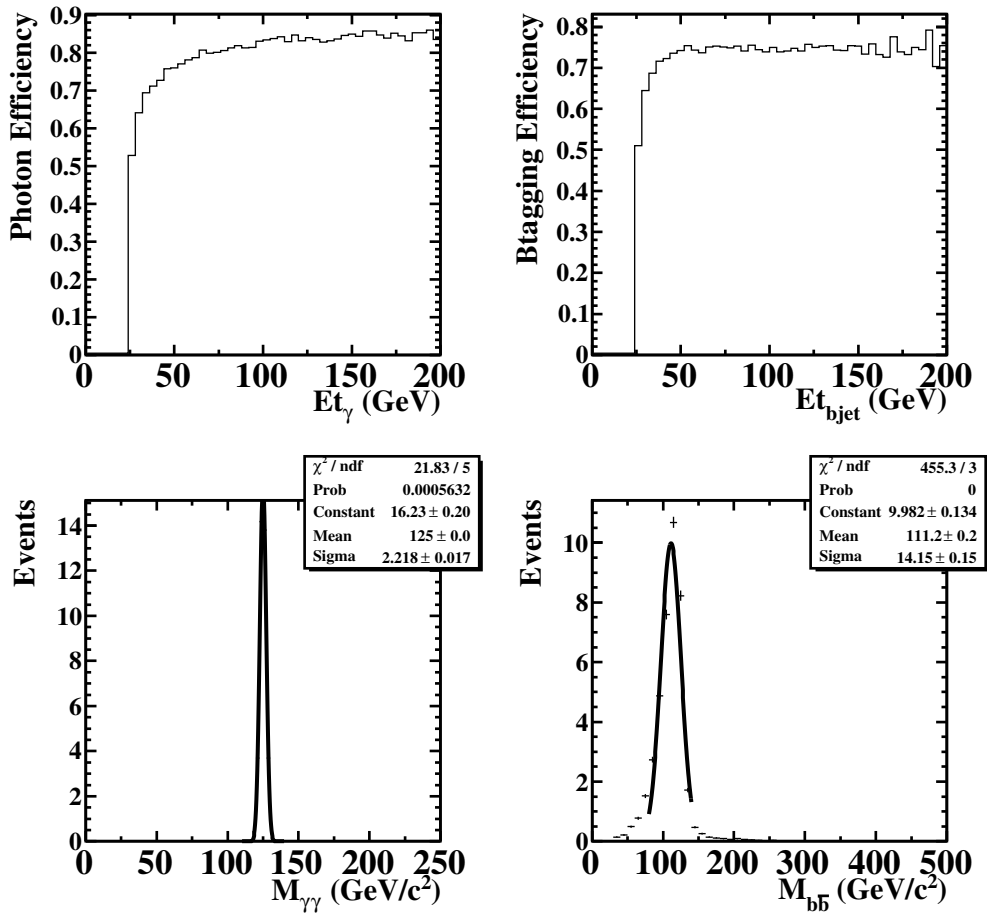


FIG. 2: The identification efficiency of photon as a function of photon  $E_t$  (upper left); the efficiency for  $b$ -jets (upper right); the invariant mass of  $H \rightarrow \gamma\gamma$  (bottom left); and the invariant mass of  $H \rightarrow b\bar{b}$  (bottom right).

The  $gg \rightarrow HH$  signal is generated using HPAIR + PYTHIA6.2 package [10]. All tree-level background processes up to 1 or 2 partons are generated using Madgraph 5 [11] + PYTHIA8.0 [12] with MLM matching [13] to avoid double counting in certain regions of phase space. The production cross section of signal and background is evaluated using the CTEQ6L parton distribution functions [14] with the corresponding value of  $\alpha_s$  at the investigated order in perturbative QCD. The signal and background processes for their cross section times branching ratio and the number of generated events are summarized in Table I for the colliders with  $\sqrt{s}=14, 33$ , and 100 TeV.

TABLE I: The signal and background processes of production cross section times branching ratio and the number of generated events for the colliders with  $\sqrt{s}=14, 33$ , and 100 TeV,

Samples	Gen. cuts	HL-LHC		TeV33		TeV100	
		$\sigma \cdot B$ (fb)	Eevent	$\sigma \cdot B$ (fb)	Events	$\sigma \cdot B$ (fb)	Events
$H(b\bar{b})H(\gamma\gamma)$		0.0892	80000	0.545	80000	3.73	80000
$b\bar{b}\gamma\gamma$	$Et_{j,b,\gamma} > 20, 20, 25$	294	1033875	1085	952811	5037	763962
$Z(b\bar{b})H(\gamma\gamma)$	$Et_{j,b,\gamma} > 20, 0, 20$	0.109	97168	0.278	82088	0.876	68585
$b\bar{b}H(\gamma\gamma)$	$Et_{j,b,\gamma} > 20, 0, 20$	2.23	120617	9.843	110663	50.49	99611
$t\bar{t}H(\gamma\gamma)$	$Et_{j,b,\gamma} > 20, 0, 20$	0.68	83491	4.76	71790	37.26	63904

### III. EVENT KINEMATICS AND SELECTIONS

The characteristic distributions of the gluon fusion process  $gg \rightarrow H \rightarrow HH$  are compared for several observables at the hadron colliders with  $\sqrt{s}=14, 33$ , and 100 TeV. In Fig. 3, we show for the Higgs pairs the normalized distributions of the transverse momentum  $Pt_H$ , the pseudorapidity  $\eta_H$ , the invariant mass  $M_{HH}$ , and the rapidity  $y_{HH}$ . They seem quite similar between the colliders so we use the common set of event selections to separate the signal from the backgrounds. The photons (npho) are required to be isolated and have  $Et > 25$  GeV and  $|\eta| < 2.5$ . The jets (njet) are required to have  $Et > 25$  GeV and  $|\eta| < 2.5$ . The  $b$ -jet candidate is a jet that has a  $b$ -tag. We select two  $b$ -jets and two photons in the final states to be consistent with the signature of  $gg \rightarrow HH \rightarrow b\bar{b}\gamma\gamma$  where each of the  $b$ -jets and photons is required to  $Et > 35$  GeV. The invariant mass of two photons is then required to be consistent within 5 GeV/ $c^2$  of  $M_H = 125$  GeV/ $c^2$  while the invariant mass of two  $b$ -jets is required to be between 85 and 135 GeV/ $c^2$ . In order to reject  $t\bar{t}$  events, we also identify the number of isolated electrons and muons (nleps) with  $Et(Pt) > 25$  and  $|\eta| < 2.5$ . If there is missing  $Et > 50$  GeV, we count nmet=1, otherwise nmet=0.

For  $H \rightarrow b\bar{b}$ , we compare the kinematic distributions between the signal and backgrounds for the sub-leading  $Pt_b$ , the  $\Delta R$  separation, the  $Pt_{b\bar{b}}$ , and the invariant mass of  $M_{b\bar{b}}$  as shown in Fig. 4. For  $H \rightarrow \gamma\gamma$ , the photon kinematic distributions are shown in Fig. 5 for the sub-leading  $Pt_\gamma$ , the  $\Delta R$  separation, the  $Pt_{\gamma\gamma}$ , and the invariant mass of  $M_{\gamma\gamma}$ . We also compare the kinematic distributions of the pair of Higgs between the signal and backgrounds for the invariant mass of  $M_{b\bar{b}\gamma\gamma}$ ,  $\Sigma(njet + npho + nlep + nmet)$ , the minimum  $\Delta R$  between the photons and the  $b$ -jets, and the  $\cos\theta_{\gamma\gamma}$ , as shown in Fig. 6.

Based on these distributions, we further apply the following cuts to optimize the sensitivity:

- $\Delta R_{\gamma\gamma} < 2.5$  and  $\Delta R_{b\bar{b}} < 2.0$
- $|\eta_{\gamma\gamma}| < 2.0$  and  $|\eta_{b\bar{b}}| < 2.0$
- $Pt_{\gamma\gamma} > 100$  and  $Pt_{b\bar{b}} > 100$  GeV
- $M_{b\bar{b}\gamma\gamma} > 300$  GeV/ $c^2$
- $|\cos\theta_H| < 0.8$ , the Higgs decay angle in the rest frame of  $HH$ .
- $\Sigma(njets + nphos + nleps + nmet) < 7$

### IV. PRELIMINARY RESULTS

After applying the event selection described above, the remaining number of signal and background events are summarized in Table II for an integrated luminosity of 3000 fb $^{-1}$ . The background seems dominated by the QCD production of  $b\bar{b}\gamma\gamma$ , which can be further reduced using a multivariate analysis technique once a realistic simulation is available.

For the high luminosity running of LHC at 14 TeV, it's possible to observe a statistical significance of 2.3  $\sigma$  signal with 3000 fb $^{-1}$  data, which is consistent with the previous studies [7]. For the higher energy colliders with  $\sqrt{s}=33$ , and 100 TeV, we would expect to observe a signal with a statistic significance of 6.2 and 15.0  $\sigma$  with 3000 fb $^{-1}$  data, respectively. In Fig. 7 - 9, we show the projections of the final invariant mass of two photons or two  $b$ -jets after selecting  $M_{b\bar{b}}$  or  $M_{\gamma\gamma}$  for  $\sqrt{s}=14, 33$ , and 100 TeV colliders, respectively. After the  $gg \rightarrow HH \rightarrow b\bar{b}\gamma\gamma$  signal is established, we would measure its production cross section and derive the Higgs self-coupling constants from the

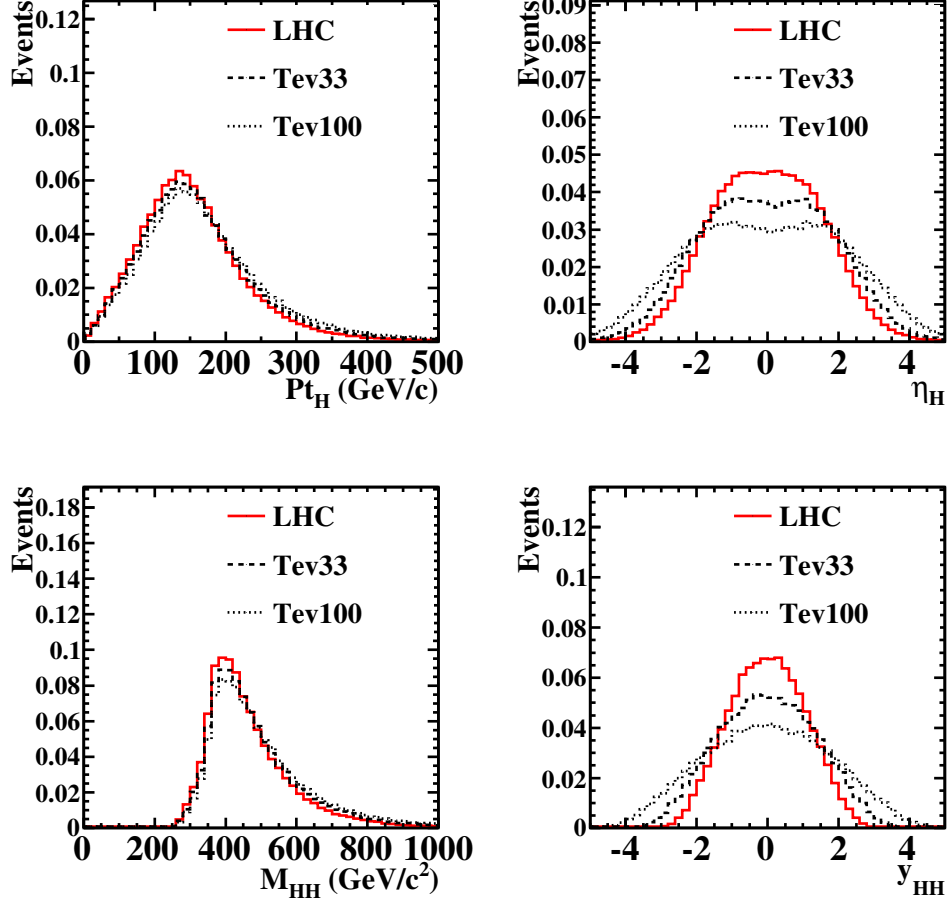


FIG. 3: The normalized distributions for  $Pt_H$ ,  $\eta_H$ ,  $M_{HH}$ , and  $y_{HH}$  at the colliders with  $\sqrt{s}=14, 33, 100$  TeV, respectively.

dependence of the  $gg \rightarrow HH$  production cross section as a function of the Higgs self-coupling constants. Based on the estimation of  $d(\sigma/\sigma_{SM})/d(\lambda/\lambda_{sm}) \approx -0.8$  from Fig. 13 in ref. [6] and the significance of  $HH \rightarrow b\bar{b}\gamma\gamma$  signal, the Higgs self-coupling can be measured to be a statistical accuracy of 50%, 20%, and 8% with  $3 \text{ ab}^{-1}$  data at the future colliders with  $\sqrt{s}=14, 33$ , and  $100$  TeV, respectively. However, it is worth to note that the event acceptance needs a correction for the dependence of Higgs self-coupling due to tight cuts used. In the future, we may have to loose some of selections while exploring kinematic distributions (shapes) that are most sensitive to the Higgs self-coupling to improve the measurement beyond simple event counting.

## V. CONCLUSION

We present a feasibility study of observing  $HH \rightarrow b\bar{b}\gamma\gamma$  at the future hadron colliders with  $\sqrt{s}=14, 33$ , and  $100$  TeV. The measured cross section then can be used to constrain the Higgs self-coupling directly in the standard model. Any deviation could be a sign of new physics. The signal and background events are estimated using Delphes 3.0.10 fast Monte Carlo simulation based on the ATLAS detector capabilities. With  $3 \text{ ab}^{-1}$  data, it would be possible to measure the Higgs self-coupling with a 50%, 20%, and 8% statistical accuracy by observing  $HH \rightarrow b\bar{b}\gamma\gamma$  at  $\sqrt{s}=14, 33$ , and  $100$  TeV colliders, respectively.

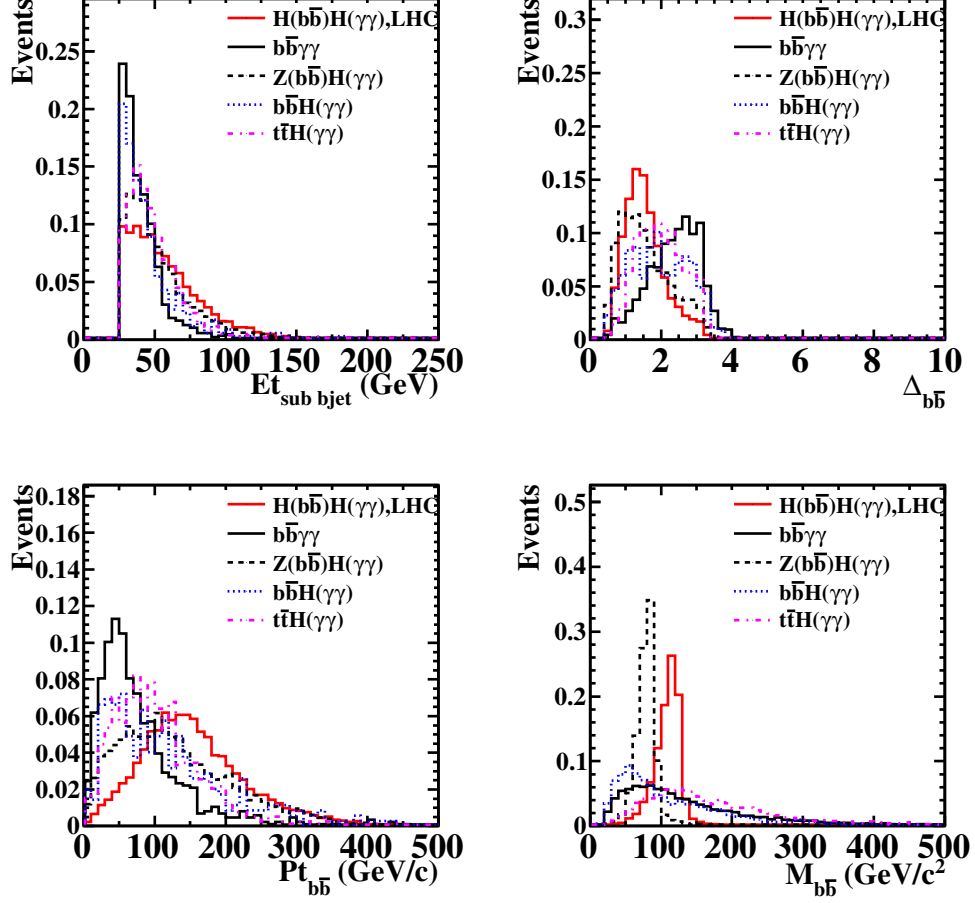


FIG. 4: The normalized distributions for the sub-leading  $b$ -jet  $E_t$ ,  $\Delta R_{b\bar{b}}$ ,  $P_{t_{b\bar{b}}}$ , and  $M_{b\bar{b}}$  from the signal and various background processes.

## VI. ACKNOWLEDGEMENT

We would like to thank C. Barrera, A. Nisati and N. Styles for their useful cross checks and valuable discussions.

- 
- [1] ATLAS Collab. (G. Aad *et al.*), *Phys. Lett. B* **716**, 1 (2012);  
CMS Collab. (S. Chatrchyan *et al.*), *Phys. Lett. B* **716**, 30 (2012).
  - [2] F. Englert and R. Brout, *Phys. Rev. Lett.* **13**, 321 (1964);  
P.W. Higgs, *Phys. Rev. Lett.* **13**, 508 (1964);  
G.S. Guralnik, C.R. Hagen, and T.W.B. Kibble, *Phys. Rev. Lett.* **13**, 585 (1964).
  - [3] M. Battaglia, E. Boos, and W. Yao, Studying the Higgs Potential at the  $e^+e^-$  Linear Collider, arXiv:hep-ph/011127.
  - [4] U. Baur, T. Plehn, and D. Rainwater, *Phys. Rev. D* **69**, 053004 (2004).
  - [5] M.J. Dolan, C. Englert and M. Spannowsky, *JHEP* **10** 112 (2012);  
F. Goertz *et al.*, *JHEP* **06** 016 (2013);  
A. Papaefstathiou, L.L. Yang, and J. Zurita, *Phys. Rev. D* **87** 011301(R) 2013.
  - [6] J. Baglio *et al.*, The measurement of the Higgs self-coupling at the LHC: theoretical status, arXiv:1212.5581.
  - [7] The ATLAS Collaboration, Studies of the ATLAS potential for Higgs self-coupling measurements at a High Luminosity LHC, ATLAS-PHYS-PUB-2013-001.
  - [8] D.Y. Shao *et al.*, *JHEP* **07**, 169 (2013).
  - [9] S. Ovin, X. Rouby and V. Lemaitre, DELPHES a framework for fast simulation of a generic collider experiment,

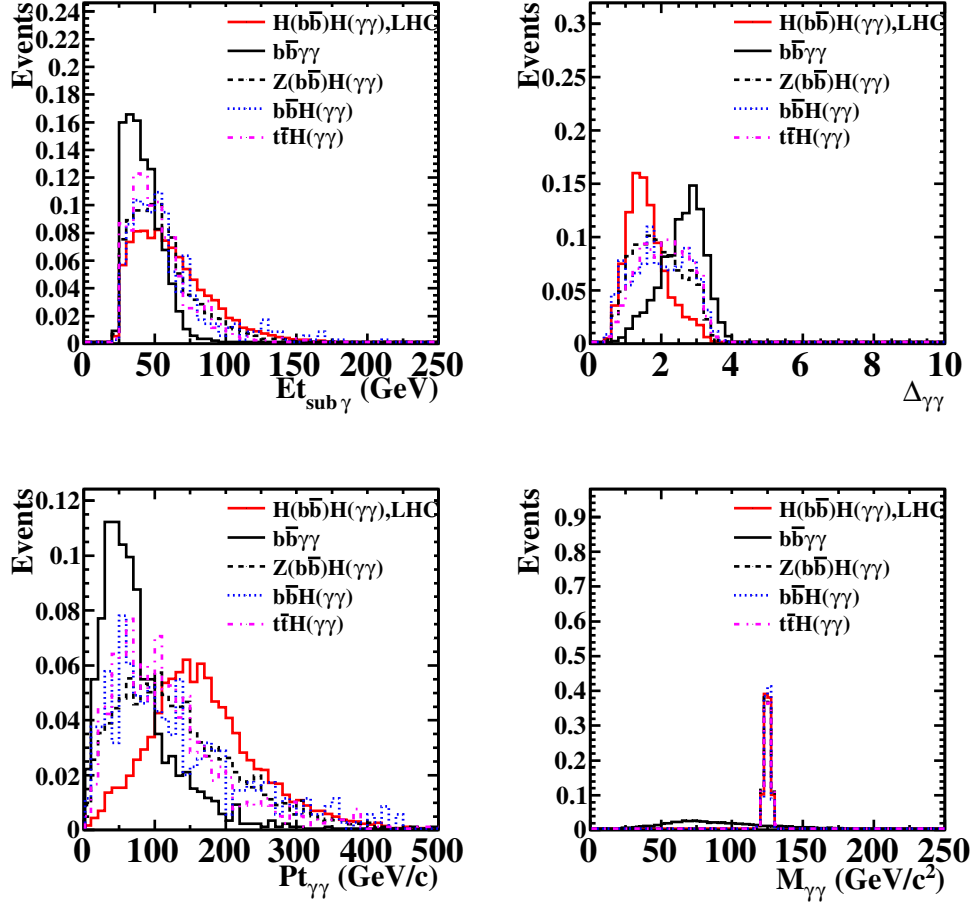


FIG. 5: The normalized distributions for the sub-leading photon  $Et$ ,  $\Delta R_{\gamma\gamma}$ ,  $Pt_{\gamma\gamma}$ , and  $M_{\gamma\gamma}$  from the signal and various background processes.

arXiv:0903.2225.

- [10] E. El Kacimi and R. Lafaye, Simulation of neutral Higgs pair production processes in PYTHIA using HPAIR matrix elements, ATL-PHYS-2002-015.
- [11] J. Alwall *et al.*, *JHEP* **1106**, 128 (2011).
- [12] T. Sjostrand, S. Mrenna, P. Skands, *Comput. Phys. Commun.* **178** 852 (2008).
- [13] M.L. Mangano *et al.*, *JHEP* **07** 001 (2003).
- [14] K. Kovarik *et al.*, CTEQ nuclear parton distribution functions, arXiv:1307.3454.

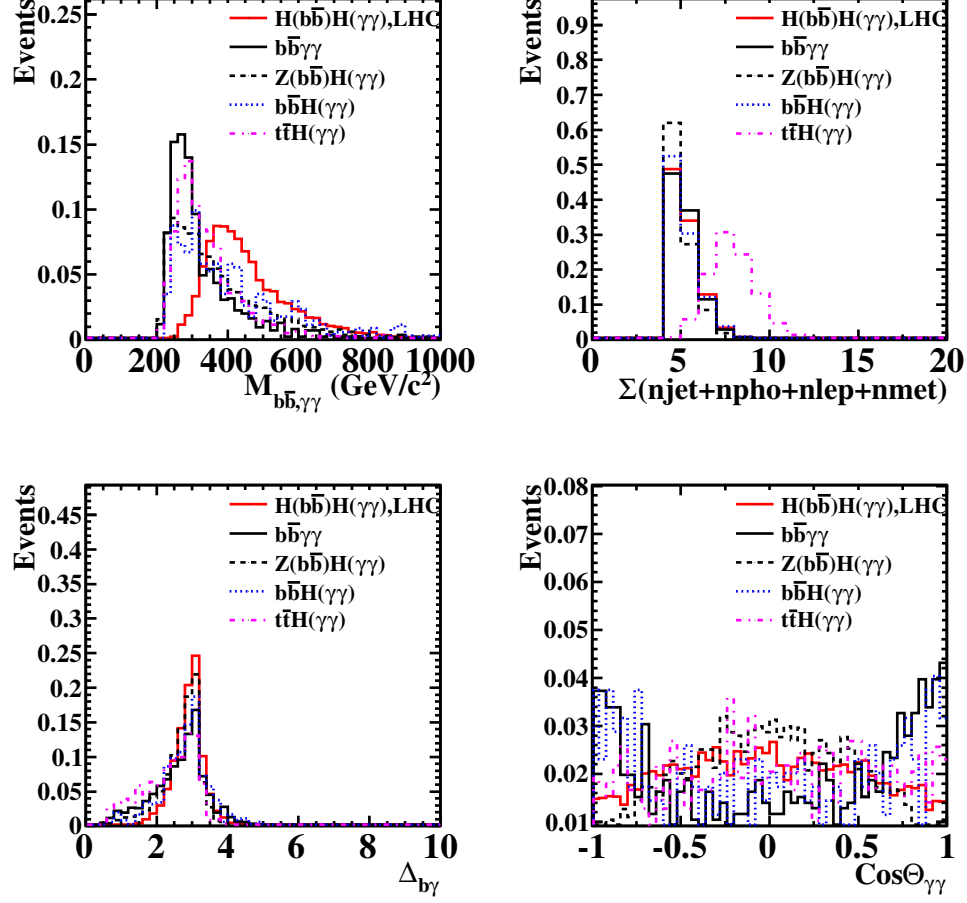


FIG. 6: The normalized distributions for  $M_{b\bar{b},\gamma\gamma}$ ,  $\Sigma(njet + npho + nlep + nmet)$ ,  $\Delta_{b\gamma,min}$ , and  $Cos\theta_{\gamma\gamma}$  from the signal and various background processes.

TABLE II: The signal and background processes of  $\sigma \times Br$ , acceptance, and the expected events with  $3000 \text{ fb}^{-1}$  data for the colliders with  $\sqrt{s}=14, 33$ , and  $100 \text{ TeV}$ .

Samples	HL-LHC (3 ab <sup>-1</sup> )			TeV33 (3 ab <sup>-1</sup> )			TeV100 (3 ab <sup>-1</sup> )		
	$\sigma \cdot Br$	Acc.	Expect	$\sigma \cdot Br$	Acc.	Expect	$\sigma \cdot Br$	Acc.	Expect
	(fb)	(%)	Evnts	(fb)	(%)	Evnts	(fb)	(%)	Evnts
HH( $b\bar{b}\gamma\gamma$ )	0.089	6.2	16.6	0.545	5.04	82.4	3.73	3.61	403.9
$b\bar{b}\gamma\gamma$	294	0.0045	40.1	1085	0.0039	126.4	5037	0.00275	415.4
$z(b\bar{b})h(\gamma\gamma)$	0.109	1.48	4.86	0.278	1.41	11.8	0.875	1.57	41.2
$b\bar{b}h(\gamma\gamma)$	2.23	0.072	4.82	9.84	0.084	24.8	50.5	0.099	150.5
$t\bar{t}h(\gamma\gamma)$	0.676	0.178	3.62	4.76	0.12	16.5	37.3	0.11	124.2
Total B	-	-	53.4	-	-	179.5	-	-	731.3
$S/\sqrt{B}$	-	-	2.3	-	-	6.2	-	-	15.0

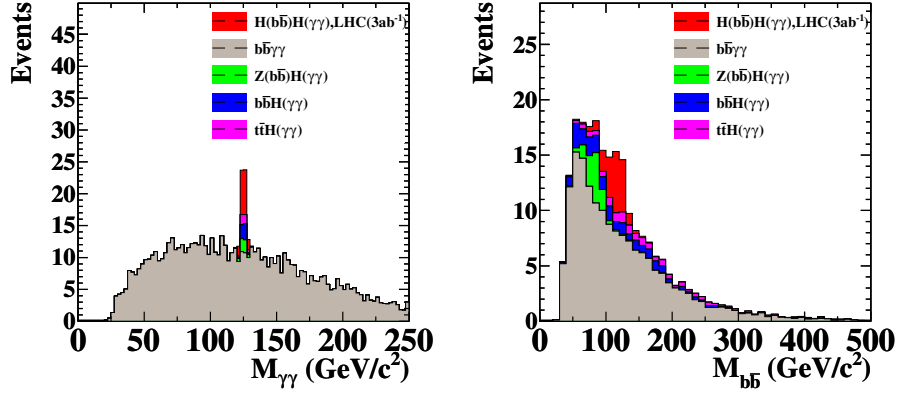


FIG. 7: The expected mass of two photons (left) or two  $b$ -jets (right) after requiring mass of two  $b$ -jets or two photons consistent with the Higgs mass at LHC with  $3000 \text{ fb}^{-1}$  data.

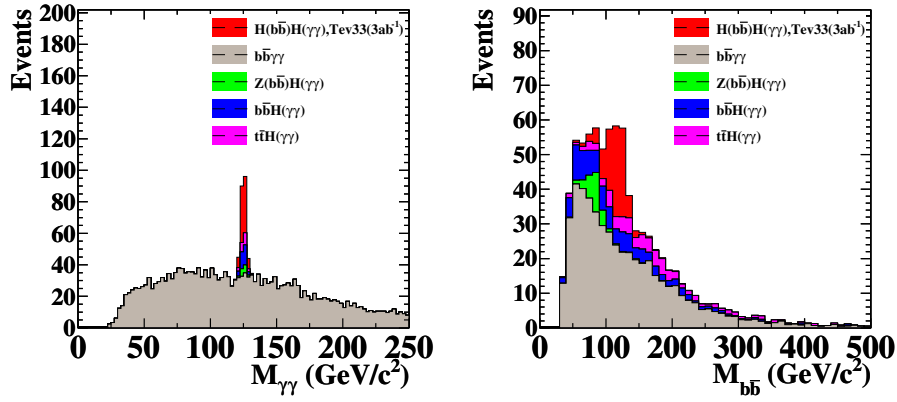


FIG. 8: The expected mass of two photons (left) or two  $b$ -jets (right) after requiring mass of two  $b$ -jets or two photons consistent with the Higgs mass at a Tev33 collider with  $3000 \text{ fb}^{-1}$  data.

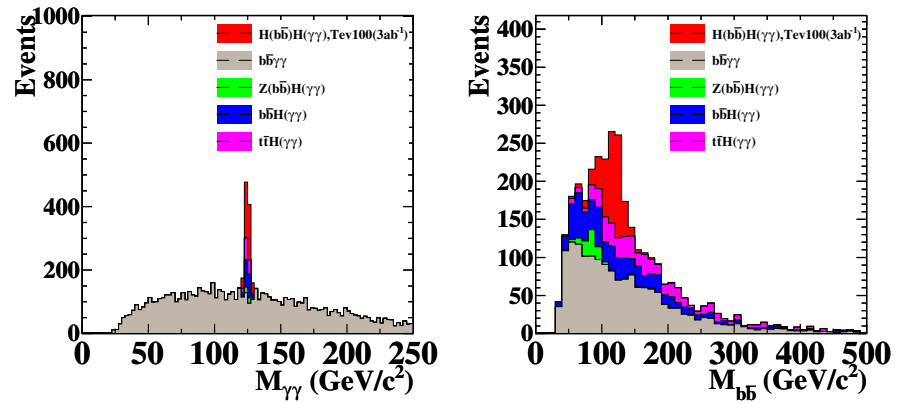


FIG. 9: The expected mass of two photons (left) or two  $b$ -jets (right) after requiring mass of two  $b$ -jets or two photons consistent with the Higgs mass at a Tev100 collider with  $3000 \text{ fb}^{-1}$  data.